

¹ **Estimating χ and K_T from fast-response using fast-response thermistors on**

² **traditional shipboard CTDs: sources of uncertainty and bias.**

³ Andy Pickering*

⁴ *College of Earth, Ocean, and Atmospheric Sciences, Oregon State University, Corvallis, OR.*

⁵ Jonathan Nash

⁶ *College of Earth, Ocean, and Atmospheric Sciences, Oregon State University, Corvallis, OR.*

⁷ James N Moum

⁸ *College of Earth, Ocean, and Atmospheric Sciences, Oregon State University, Corvallis, OR.*

⁹ Jen MacKinnon

¹⁰ *UCSD / Scripps Institute of Oceanography*

¹¹ *Corresponding author address: College of Earth, Ocean, and Atmospheric Sciences, Oregon State University, Corvallis, OR.

¹² E-mail:

ABSTRACT

14 The acquisition of turbulence data from traditional shipboard CTD casts is
15 attractive, as it has the potential to significantly increase the amount of deep-
16 ocean mixing observations globally. While data from shear-probes are eas-
17 ily contaminated by motion of the instrument platform, the measurement of
18 temperature gradient is relatively insensitive to vehicle vibration, making it
19 possible to measure temperature gradient from a shipboard CTD rosette. The
20 purpose of this note is to investigate the error and bias in estimating the rate
21 of dissipation of temperature variance χ and turbulent diffusivity K_T from
22 thermistors mounted on traditional CTD casts. The most significant source
23 of error is associated with the fact that fast-response FP07 thermistors resolve
24 only a fraction of the temperature gradient variance at the fallspeed of typi-
25 cal CTD casts. Assumptions must be made about the wavenumber extent of
26 the temperature gradient spectrum, which scales with the rate of dissipation
27 of turbulent kinetic energy, a quantity that is not directly measured. Here we
28 utilize observations from a microstructure profiler to demonstrate the validity
29 of our method of estimating χ from thermistor data, and to assess uncertainty
30 and bias. We then apply this methodology to temperature gradient profiles ob-
31 tained from χ pods mounted on a CTD (the CTD- χ pod), and compare these
32 to microstructure profiles obtained almost synoptically at the equator. CTD-
33 χ pod estimates of χ compare favorably to the direct microstructure measure-
34 ments and demonstrate that the χ pod method is not significantly biased. This
35 supports the utility of the measurement as part of the global repeat hydrog-
36 raphy program (GO-SHIP) cruises, during which this type of data has been
37 acquired during the past few years.

³⁸ **1. Introduction**

³⁹ Turbulent mixing affects the distribution of heat, salt, and nutrients throughout the global ocean.

⁴⁰ Diapycnal mixing of cold, dense water with warmer water above maintains the abyssal overturning

⁴¹ circulation (Munk 1966; Munk and Wunsch 1998), which affects global climate. Because the

⁴² turbulence that drives mixing generally occurs at scales that are not resolved in climate models,

⁴³ it must be parameterized, based on either (i) aspects of the resolved model dynamics, (ii) through

⁴⁴ higher resolution models that capture the dynamics that feed energy to turbulence, or (iii) using

⁴⁵ other parameterizations that either dynamically or statistically quantify turbulent fluxes. Recent

⁴⁶ investigations have demonstrated that these models are sensitive to the magnitude and distribution

⁴⁷ of mixing (Melet et al. 2013). A comprehensive set of measurements that spans relevant dynamical

⁴⁸ regimes is needed to constrain mixing and develop more accurate parameterizations.

⁴⁹ Direct measurement of mixing with microstructure profilers equipped with shear probes is

⁵⁰ well-suited for targeting upper-ocean processes. However, this technique can be expensive, time-

⁵¹ intensive, and requires considerable care and expertise. Moreover, tethered profilers can't reach

⁵² abyssal depths, requiring autonomous instruments to get deeper than \sim 1000-2000 m. As a result,

⁵³ existing measurements of diapycnal mixing, especially in the deep ocean, are sparse (Waterhouse

⁵⁴ et al. 2014). In order to obtain a larger quantity of mixing estimates, considerable work has gone

⁵⁵ into inferring mixing from measurements of the outer scales of turbulence, which are easier to

⁵⁶ obtain. One popular method is the use of Thorpe scales, where diapycnal mixing is inferred from

⁵⁷ inversions in profiles of temperature or density (Thorpe 1977; Dillon 1982). The size of resolv-

⁵⁸ able overturn is limited by the profiling speed and instrument noise (Galbraith and Kelley 1996).

⁵⁹ ~~Several~~ While some studies indicate relatively good agreement with microstructure and other ob-

⁶⁰ servations, ~~but there are some~~ there remain questions about the general validity of the method

and the assumptions made (Mater et al. 2015; Scotti 2015). Parameterizations based on profiles of shear and/or strain have also been developed and applied to estimate diapycnal mixing (Gregg 1989; Kunze et al. 2006; Polzin et al. 2013; Whalen et al. 2012, 2015). However, they rely on a series of assumptions about the cascade of energy from large to small scales that are often violated; numerous studies (i.e., Waterman et al. (2013)) have shown that there is significant uncertainty associated with these parameterizations, in that there can be a consistent bias in a particular region, yet the sense of the bias (i.e., overpredict vs. underpredict) is not known a priori.

Quanitifying turbulence from velocity shear variance (to compute the dissipation rate of turbulent kinetic energy ε) is challenging on moorings or profiling platforms because there is usually too much vibration and/or package motion for shear-probes to be useful. Pitot-static tubes have recently been used for this purpose, plus providing independent measurements of speed (Moum 2015). Other methods (i.e., optics or acoustics) may hold some promise, but lack of scatterers often precludes this type of measurement, especially in the abyss. In addition, shear probes only provide ε , not the mixing of scalars, K , which is often inferred from ε by assuming a mixing efficiency Γ (Osborn 1980) as $K = \Gamma\varepsilon/N^2$, which where N^2 is the buoyancy frequency. A more direct measure of turbulent mixing is obtained from the dissipation rate of temperature variance χ (Osborn and Cox 1972). This has the advantage that (i) the temperature and temperature gradient can be computed and are relatively straightforward to measure, and (ii) the estimation of mixing from χ does not require assumptions about Γ . However, the spectrum of temperature gradient extends to very small scales, so that its spectrum is seldom fully resolved (and unlike shear variance, the wavenumber extent of the temperature gradient spectrum does not scale with its amplitude, but instead depends on ε). Assumptions about the spectral shape (Kraichnan vs. Batchelor, and the value of the “constant” q) and its wavenumber extent (governed by the Batchelor wavenumber $k_b = [\varepsilon/(vD_T^2)]^{1/4}$ (Batchelor 1959)) are thus necessary to determine χ unless measurements

capture the full viscous-diffusive subrange of turbulence (i.e., down to scales $\Delta x \sim 1/k_b \sim 1\text{mm}$), a criterion seldom achieved. To resolve this, we follow Alford and Pinkel (2000) and Moum and Nash (2009) and make the assumption that $K_T = K_p$ to determine the dissipation rate as $\varepsilon_\chi = (N^2 \chi) / (2\Gamma \langle dT/dz \rangle^2)$, permitting estimation of k_b to be estimated.

The goal of this paper is to outline and validate the methods used to compute χ and K_T with χ -pods mounted on CTDs (Figure 1). We do this by applying our processing methodology to profiles of temperature gradient measured by thermistors on the ‘Chameleon’ microstructure profiler, which provides a direct test of our methodology. Because Chameleon is a loosely tethered profiler equipped with shear probes (Moum et al 1995), it directly measures ε and allows us to test our assumptions. Specifically, it allows us to determine biases associated with computing χ from partially-resolved temperature gradient spectra alone, as compared to that when it is computed by including knowledge of the dissipation rate computation that includes ε , which constrains the wavenumber extent of the scalar spectra. After establishing that the method works, we then compare CTD- χ pod profiles to nearby microstructure profiles.

2. Data

a. EQ14

Data were collected on the R/V Oceanus in Fall 2014 during the EQ14 experiment to study equatorial mixing. More than 2700 Chameleon profiles were made, along with 35 CTD- χ pod profiles bracketed by Chameleon profiles in order to maintain calibrations during the cruise. Most Chameleon profiles were made to a maximum depth of about 250m, with CTD casts going to 500m or deeper. The EQ14 experiment and results are discussed in more detail in (SJ Warner, RN

¹⁰⁶ Holmes, EH McHugh-Hawkins, JN Moum, 2016: Buoyant gravity currents released from tropical
¹⁰⁷ instability waves, JPO, in preparation) [and Holmes et al. \(2016\)](#).

¹⁰⁸ **3. Methods**

¹⁰⁹ As mentioned in the introduction, the temperature gradient spectrum is rarely fully resolved
¹¹⁰ down to the small scales of turbulent mixing. The fraction of the spectrum resolved depends on
¹¹¹ the true spectrum (a function of χ and ε), the flowspeed past the sensor (u), and the response of
¹¹² the thermistor. The GE/Thermometrics FP07 thermistors we use typically resolve frequencies up
¹¹³ to about $f_{max} = 10 - 15$ Hz. The maximum resolved wavenumber is then equal to $k_{max} = f_{max}/u$,
¹¹⁴ while the wavenumber extent of the true spectrum varies with k_b (and $\varepsilon^{1/4}$). At the typical vertical
¹¹⁵ fall rate of a CTD rosette (~ 1 m/s), only about 20% of k_b is resolved at $\varepsilon = 10^{-10} \text{ W kg}^{-1}$ (Figure
¹¹⁶ 2). While methods have been developed to fit the observed temperature gradient spectrum to
¹¹⁷ theoretical forms (Ruddick et al. 2000), these work only when a larger fraction of the temperature
¹¹⁸ gradient spectrum is resolved. For the relatively high profiling speeds typical of CTD casts, we
¹¹⁹ find these methods do not work well (see appendix for details) and therefore we use the following
¹²⁰ methodology, which does not have a strongly ε -dependent bias.

¹²¹ We first outline our method for estimating χ , which relies on (i) determining the instantaneous
¹²² flowspeed past the sensor, (ii) identifying periods where the signals may be contaminated by the
¹²³ wake of the CTD rosette, (iii) defining the ~~relavent~~ [relevant values of](#) N^2 and $(dT/dz)^2$, and (iv)
¹²⁴ applying an iterative method to compute χ ~~and~~ [KT](#). We then discuss some limitations and practical
¹²⁵ considerations that arise.

¹²⁶ a. Iterative Method for estimating χ

¹²⁷ For each ~ 1 second window, χ is estimated via the following procedure as outlined in Moum
¹²⁸ and Nash (2009). For isotropic turbulence,

$$\chi_T = 6D_T \int_0^\infty \Psi_{T_x}(k) dk \quad (1)$$

¹²⁹ where D_T is the thermal diffusivity and $\Psi_{T_x}(k)$ is the wavenumber spectrum of dT/dx .

¹³⁰ Note that dT/dx is not actually measured; dT/dt is measured, and dT/dx is inferred from
¹³¹ Taylor's frozen flow hypothesis:

$$\frac{dT}{dx} = \frac{1}{u} \frac{dT}{dt} \quad (2)$$

¹³² where u represents the flow speed past the sensor. The wavenumber extent of the spectrum
¹³³ depends on the Batchelor wavenumber k_b , which is related to ε :

$$k_b = [\varepsilon / (v D_T^2)]^{1/4} \quad (3)$$

¹³⁴ We assume that $K_\rho = K_T$ and $K_\rho = \Gamma \varepsilon / N^2$ where Γ is the mixing efficiency, assumed to be 0.2
¹³⁵ (Moum and Nash 2009). Then dissipation rate is computed as

$$\varepsilon_\chi = \frac{N^2 \chi_T}{2\Gamma \langle dT/dz \rangle^2} \quad (4)$$

¹³⁶ Typical thermistors do not resolve the spectrum out to k_b , so the measured spectrum is fit to the
¹³⁷ Kraichnan form of theoretical scalar spectrum over the range of resolved wavenumbers ($k_{min} <$
¹³⁸ $k < k_{max}$). The variance between the measured $[\Phi_{T_x}(k)]_{obs}$ and theoretical $[\Phi_{T_x}(k)]_{theory}$ spectra at
¹³⁹ these wavenumbers is assumed to be equal:

$$\int_{k_{min}}^{k_{max}} [\Phi_{T_x}(k)]_{obs} dk = \int_{k_{min}}^{k_{max}} [\Phi_{T_x}(k)]_{theory} dk \quad (5)$$

¹⁴⁰ An iterative procedure is then used to fit and calculate χ and ε :

141 1. First we estimate χ_T based on an initial guess of $\varepsilon = 10^{-7}$ Wkg⁻¹ and compute k_b via eq. 3.

142 We set $k_{max} = k_b/2$ or to a wavenumber equivalent to $f_{max} = 7$ Hz [i.e., $k_{max} = 2\pi(f_{max})/u$],
143 whichever is smaller. In general f_{max} should be the highest value which is safely below the
144 sensor's roll-off. We chose $f_{max} = 7$ Hz in this case based on inspection of the temperature
145 gradient spectra and historical measurements of these sensors (see appendix for more details).

146 2. We then use Eq. (4) to refine our estimate of ε and k_b and recompute χ_T using Eqs. (1) and
147 (5).

148 3. This sequence is repeated and converges after two or three iterations.

149 Note that this procedure is equivalent to the explicit formulation of (Alford and Pinkel 2000),
150 except we use the Kraichnan theoretical form instead of the Batchelor spectrum for $[\Phi_{T_x}(k)]_{theory}$.

151 At wavenumbers below the spectral peak, there is little distinction between the Kraichnan and
152 Batchelor spectra, so this factor does not affect the computational bias.

153 b. CTD- χ pod Data Processing

154 The We next review the basic outline for processing each CTD- χ -pod profile is as follows: pod
155 profile. The moored χ pod instrument (Moum and Nash 2009) has a pressure sensor, compass, and
156 pitot-static tube. In contrast, the CTD- χ pod requires pressure measured by the CTD and has no
157 independent speed measurement other than dp/dt from the CTD.

158 1. The correct time-offset for the χ -pod-pod clock is determined by aligning highpass-filtered
159 dp/dt from the 24Hz CTD data to integrated vertical accelerations measured by the
160 χ -pod-pod. χ -pod-pod clock drift is small, typically on the order of 1 sec/week, but it is
161 imperative to get records aligned within < 0.5 s so that the correct $u=w=dp/dt$ value of u

162 is used. In the case of the CTD- χ pod we assume u is solely due to the vertical motion of the
163 CTD cage, i.e. $u = dp/dt$.

164 2. Low-order polynomial calibration coefficients are determined to convert thermistor voltages
165 from χ pod to ITS90 temperature (as measured by the CTD). Figure 3 shows an example of
166 the aligned and calibrated CTD- χ pod timeseries for one cast. Note the significant differences
167 in amount of variance associated with the two sensors during down and up casts. For the
168 upward-mounted sensor (T1), the downcast signal is largely associated with the CTD wake,
169 as is the upcast for the downward-mounted sensor (T2). Only the ‘clean’ portions of the cast
170 (e.g., the T1 upcast and the T2 downcast) are used in the χ pod calculations.

171 3. Depth loops are identified and flagged in the 24Hz CTD data Figure 4. χ -~~pod~~- χ pod data
172 during these times are discarded since the signals are likely contaminated by the wake of the
173 CTD. We use a ~~vertical~~- χ pod velocity threshold of 0.3m/s and throw out data within 2m
174 of the identified loops. Even for profiles that are significantly affected by ship heaving, good
175 segments of data are obtained over a majority of the depths after removing contaminated data,
176 allowing us to compute values in nearly every 10m bin.

177 4. Buoyancy frequency N^2 and temperature gradient dT/dz are computed from 1-m binned
178 CTD data, and averaged over a scale of 10m. The results are not very sensitive to the averag-
179 ing interval (see appendix for more details).

180 5. Half-overlapping 1 sec windows of data are used to estimate χ and K_T following the methods
181 described in Moum and Nash (2009), as outlined in the previous section.

182 c. Example Spectra and Fits

183 Examples of the observed and fit spectra are shown in Figure 5, for low and high dissipation
184 rate. Note that at lower ϵ , a larger fraction of k_b is observed and the peak of the spectrum is
185 nearly almost resolved. At higher ϵ , less of the spectrum is resolved and the spectral peak is
186 well above the maximum resolved wavenumber. Even so, the iterative χ pod method gives an
187 accurate estimate of χ . The χ pod and Chameleon fits are performed over the same wavenumber
188 range and match there. However, the higher-wavenumber portions of the fit spectra differ since
189 the Chameleon fits use the observed k_b to determine the wavenumber extent.

190 d. *flowspeed past the sensor*

191 The flowspeed past the thermistor is needed to convert the measured temperature derivative
192 dT/dt to a spatial gradient. For the CTD χ pod, the largest contribution to the flowspeed is
193 usually the vertical velocity of the CTD package (dp/dt), which is close to 1 m/s on average,
194 so we typically neglect the horizontal component of velocity in converting from frequency to
195 wavenumber spectra. Although usually a good approximation, errors may be introduced where
196 horizontal velocities are large. Note that because it is the total instantaneous velocity magnitude
197 that represents flow past the sensor, neglecting the horizontal component of velocity (assuming
198 $u = dp/dt$) means we are always underestimating the true flowspeed past the sensor. When the
199 CTD package is equipped with LADCP, the true flowspeed can be measured. In some cases
200 (including EQ14) where the CTD was not equipped with LADCP, it would seem that the ship's
201 ADCP could be used to estimate the horizontal component of velocity. However, because the CTD
202 does not travel perfectly vertically in strong currents, this is difficult to do in practice. In a strong
203 horizontal flow, the CTD will drift with the current while descending, lowering the flow relative
204 to the sensors. On the upcasts, the CTD will be pulled against the current, increasing the flow

205 relative to the sensors. Since the CTD in EQ14 was not equipped with LADCP, we use dp/dt as
206 the flowspeed, and estimate potential errors in the appendix.

207 4. Results

208 a. Direct Test of χ_{pod} Method

209 We begin by utilizing the highly-resolved turbulence profiler data from the freely-falling
210 turbulence profiler, Chameleon (for which both ε and χ are measured) to test the assumptions in
211 our method of estimating χ . We first apply the χ_{pod} method to each Chameleon profile, using
212 only the FP07 thermistor data. These results, which we will refer to as χ_{χ}^{cham} and assume no
213 independent knowledge of ε , are then compared with $\chi_{\varepsilon}^{cham}$, computed by integrating the theo-
214 retical temperature gradient spectrum with where k_b is computed directly from shear-probe derived
215 ε . Qualitatively, χ_{χ} and χ_{ε} show very similar depth and time patterns (Figure
216 6) and appear to agree in magnitude, suggesting the method works well. A more quantitative
217 comparison is made with a 2-D histogram (Figure 7), showing shows the two are well-correlated
218 over a wide range of magnitudes five orders of magnitude. The distribution of \log_{10} of the χ ratios
219 is approximately normal, with a mean of $\mu = -0.1$ and standard deviation of $\sigma = 0.51$. This
220 indicates a low bias of χ_{χ}^{cham} relative to $\chi_{\varepsilon}^{cham}$ of 20% and random variation of a factor of 3.

221 b. CTD χ_{pod} -Chameleon Comparison

222 Having demonstrated that the method works using Chameleon data, we now compare χ_{χ}^{ctd}
223 from CTD-mounted χ_{pods} to $\chi_{\varepsilon}^{cham}$. In contrast to the Chameleon data, the CTD is more
224 strongly coupled to the ship, and therefore subject to more vibration, heaving, and artificial tur-
225 bulence created by the rosette. A total of 35 CTD- χ_{pod} casts were performed, bracketed with
226 Chameleon profiles immediately before and after. We first compare CTD- χ_{pod} profiles to the

mean of the two Chameleon profiles bracketing each cast, both averaged in 5m depth bins (Figure 8). The two are correlated, with considerable scatter. A histogram of the log of ratios is approximately normal and has a mean of -0.31 , indicating a possible small negative bias. Since we expect significant natural variability even between adjacent Chameleon profiles, we investigate further to determine if the observed χ pod variability is of a similar magnitude or greater than expected. Scatter plots of before vs. after Chameleon profiles (not shown), typically separated by about an hour, show a similar level of scatter as the differences between methods, suggesting that the observed differences (Figure 8) can be explained by natural variability in turbulence. This is demonstrated by histograms of the ratio of χ from adjacent casts (Figure 9) which show that the variability between CTD χ pod and Chameleon casts is similar to the natural variability between before/after Chameleon profiles. Profiles from all CTD-Chameleon pairs averaged in time and 40m depth bins (Figure 10) overlap within 95% confidence limits at all depths where there exists good data for both. Averages of subsets of these profiles that were clustered in position/time (not shown) also agree well. We conclude that the variability between CTD χ pod and Chameleon profiles is indistinguishable from natural variability in turbulence levels.

5. Discussion

We have shown that χ can be accurately estimated from χ pods attached to CTD rosettes. The method also estimates ε , but we have not discussed it here since it involves more assumptions and uncertainties. One major assumption is the mixing efficiency Γ . A value of 0.2 is commonly assumed, but evidence suggests this may vary significantly. Moum and Nash (2009) found a bias of up to 1.6 for Γ values ranging from 0.1 to 0.35. Another major assumption in the χ pod method is that $K_T = K_\rho$. ~~Preliminary investigation on this data suggests that this assumption does not~~

~~hold here and may be responsible for a negative bias in ϵ , but more work is needed to verify this.~~
~~However we have shown that even if ϵ estimates are biased, χ and K_T are still robust.~~

The goal of CTD- χ pods is to expand the number and spatial coverage of ocean mixing observations. We have already deployed instruments during several process experiments and on several GO-SHIP repeat-hydrography cruises. We plan to continue regular deployment on GO-SHIP and similar cruises, adding χ ~~and K_T~~ to the suite of variables regularly measured. The expanding database of mixing measurements from CTD- χ pods will also enable testing of other commonly-used or new mixing parameterizations. This has the potential to be transformative for the field, allowing the community to develop and test global turbulence parameterizations, use estimates of turbulence along with the CLIVAR repeat hydrography data for inverse models and water mass modification calculations, identify hotspots of turbulence to target with future process experiments, and compare with in-situ chemical and biological measurements made routinely on repeat hydrography cruises.

6. Conclusions

- The χ pod method for estimating χ ~~and K_T~~ was directly applied to temperature gradients measured by the Chameleon microstructure profiler on > 2700 profiles during the EQ14 cruise. The estimated χ_χ agrees well with χ_ϵ calculated using ϵ from shear probes over a wide range of magnitudes (Figure 7) with little or no bias, demonstrating that the method works.
- CTD- χ pod profiles were also compared to nearby Chameleon profiles during the cruise. Variability between CTD- χ pod and Chameleon estimates of χ is indistinguishable from natural variability between Chameleon profiles. Time-averaged profiles of χ from both platforms

271 agree within 95% confidence limits, and no significant bias was detected between the esti-
272 mates of χ .

- 273 • We conclude that estimates of χ ~~and K_T~~ made from the CTD- χ pod platform are robust and
274 reliable.

275 *Acknowledgments.* The EQ14 experiment was funded by ~~??? budget (NSF?) 1256620~~. We thank
276 the Captain and crew of R/V Oceanus. ~~Also thank people who helped collect the data, those who~~
277 ~~Pavana Vutukur, Craig Van Appledorn, Mike Neeley-Brown~~ made the sensors,~~etc.~~ . ~~Aurelie~~
278 ~~Moulin, Ryan Holmes, Sally Warner and Anna Savage helped to collect the data.~~

279 APPENDIX A

280 **Sensitivity Analysis**

281 **A1. Flowspeed Past Sensor**

282 To quantify the potential error in the χ pod calculations from ignoring horizontal velocities
283 and assuming the flow speed is equal to the vertical speed of the CTD rosette, we repeated the
284 calculations with constant offsets added to the flowspeed. ~~Since Note that since~~ the total magnitude
285 of velocity is used, dp/dt is a minimum estimate of the true speed. Adding 0.1(1)m/s results in a
286 mean percent error of 14(58) percent (Figure 11), small compared the large natural variability in
287 turbulence and uncertainty in our measurements. Note that increasing the velocity tends to result
288 in smaller values of χ , since it shifts the spectrum to lower wavenumbers.

289 We also looked for any systematic biases associated with flowpseed. We found the χ was biased
290 high for very small speeds ($u < 25\text{cm/s}$). This could be assoicated with contamination by CTD
291 wake or entrained water when the CTD slows. These values were discarded for our analysis.

292 **A2. N^2 and dT/dz**

293 We investigated the sensitivity of the calculations to the scale over which N^2 , dT/dz are aver-
294 aged. The iterative method to estimate chi requires the background stratification N^2 and tempera-
295 ture gradient dT/dz . The estimate of χ is insensitive to these scales. However, while dissipation
296 rate ε and diffusivity K_T are more strongly affected because they are linearly related to these val-
297 ues. Computing N^2 and dT/dz over smaller scales (less than a few m) results in larger values and
298 hence some larger values of K_T .

299 **APPENDIX B**

300 **Test of MLE fitting method**

301 We also tested the spectrum fitting method of Ruddick et al. (2000) and compared to our χ_{pod}
302 method. The MLE method works well and gives similar results to our method at true ε values
303 less than about 10^{-9} , but severely underestimates χ at larger values of epsilon, where only a small
304 fraction of the spectrum is resolved (Figure 12). At lower profiling speeds we would expect the
305 MLE method to work better, as more of the spectrum will be resolved for a given value of *epsilon*.

306 **APPENDIX C**

307 **Thermistor Frequency Response**

308 Prior to 2009, the transfer function for each FP07 thermistor was measured by profiling adjacent
309 to a thermocouple in Yaquina Bay, OR. However, measuring the transfer function for each indi-
310 vidual thermistor proved too expensive and time-consuming, and since that time a generic transfer
311 function has been used. Figure 13 shows the measured transfer functions for 2008. The majority
312 of the *the*-transfer functions are similar for *at*-frequencies up to about 10 Hz, and begin to sig-

313 nificantly differ above that. To estimate the potential error in not using a transfer function, we
314 calculated the % of spectral variance captured for each of the measured functions. For frequencies
315 up to 7Hz, more than 95% is captured for 88% of the measured functions. If frequencies up to
316 15hz are used, more than 95 % variance is captured only 67% of the time. Using only frequencies
317 up to 7Hz (where the transfer function is equal to or very close to unity) avoids the issue of the
318 unknown transfer functions.

319 References

- 320 Alford, M., and R. Pinkel, 2000: Patterns of turbulent and double diffusive phenomena: Observa-
321 tions from a rapid profiling conductivity probe. *J. Phys. Oceanogr.*, **30**, 833–854.
- 322 Batchelor, G. K., 1959: Small-scale variation of convected quantitites like temperature in turbulent
323 fluid. *J. Fluid Mech.*, **5**, 113–139.
- 324 Dillon, T. M., 1982: Vertical overturns: A comparison of Thorpe and Ozmidov length scales. *J.*
325 *Geophys. Res.*, **87**, 9601–9613.
- 326 Galbraith, P. S., and D. E. Kelley, 1996: Identifying overturns in CTD profiles. *J. Atmos. Ocean.*
327 *Tech.*, **13**, 688–702.
- 328 Gregg, M., 1989: Scaling turbulent dissipation in the thermocline. *J. Geophys. Res.*, **94 (C7)**,
329 9686–9698.
- 330 Holmes, R., J. Moum, and L. Thomas, 2016: Evidence for seafloor-intensified mixing by surface-
331 generated equatorial waves. *Geophysical Research Letters*, **43 (3)**, 1202–1210.
- 332 Kunze, E., E. Firing, J. Hummon, T. K. Chereskin, and A. Thurnherr, 2006: Global abyssal mixing
333 inferred from lowered ADCP shear and CTD strain profiles. *Journal of Physical Oceanography*,
334 **36 (8)**, 1553–1576.

- 335 Mater, B. D., S. K. Venayagamoorthy, L. S. Laurent, and J. N. Moum, 2015: Biases in Thorpe scale
336 estimates of turbulence dissipation Part I: Assessments from large-scale overturns in oceanographic
337 data. *J. Phys. Oceanogr.*, **45** (2015), 2497–2521.
- 338 Melet, A., R. Hallberg, S. Legg, and K. L. Polzin, 2013: Sensitivity of the ocean state to the
339 vertical distribution of internal-tide-driven mixing. *J. Phys. Oceanogr.*, **43** (3), 602–615, doi:
340 <http://dx.doi.org/10.1175/JPO-D-12-055.1>.
- 341 Moum, J., and J. Nash, 2009: Mixing measurements on an equatorial ocean mooring. *J. Atmos.*
342 *Ocean. Tech.*, **26**, 317–336.
- 343 Moum, J. N., 2015: Ocean speed and turbulence measurements using pitot-static tubes on moorings. *Journal of Atmospheric and Oceanic Technology*, (2015).
- 344 Munk, W., and C. Wunsch, 1998: Abyssal recipes II: energetics of tidal and wind mixing. *Deep-Sea Res. Part I*, **45**, 1977–2010.
- 345 Munk, W. H., 1966: Abyssal recipes. *Deep-Sea Res.*, **13**, 707–730.
- 346 Osborn, T. R., 1980: Estimates of the local rate of vertical diffusion from dissipation measurements. *J. Phys. Oceanogr.*, **10**, 83–89.
- 347 Osborn, T. R., and C. S. Cox, 1972: Oceanic fine structure. *Geophys. Fluid Dyn.*, **3**, 321–345.
- 348 Polzin, K. L., A. C. Naveira Garabato, T. N. Huussen, B. M. Sloyan, and S. N. Waterman, 2013:
349 Finescale parameterizations of turbulent dissipation. *Rev. Geophys.*, **submitted**.
- 350 Ruddick, B., A. Anis, and K. Thompson, 2000: Maximum likelihood spectral fitting: The Batchelor
351 spectrum. *J. Atmos. Ocean. Tech.*, **17**, 1541–1555.

- 355 Scotti, A., 2015: Biases in Thorpe scale estimates of turbulence dissipation Part II: Energetics
356 arguments and turbulence simulations. *J. Phys. Oceanogr.*, **45** (2015), 2522–2543.
- 357 Thorpe, S., 1977: Turbulence and mixing in a Scottish Loch. *Philos. Trans. R. Soc. London Ser.*
358 **A**, **286**, 125–181.
- 359 Waterhouse, A. F., and Coauthors, 2014: Global patterns of diapycnal mixing from measurements
360 of the turbulent dissipation rate. *J. Phys. Oceanogr.*, **44** (7), 1854–1872.
- 361 Waterman, S., A. C. N. Garabato, and K. L. Polzin, 2013: Internal waves and turbulence in the
362 antarctic circumpolar current. *Journal of Physical Oceanography*, **43** (2), 259–282.
- 363 Whalen, C. B., J. A. MacKinnon, L. D. Talley, and A. F. Waterhouse, 2015: Estimating the
364 mean diapycnal mixing using a finescale strain parameterization. *Journal of Physical Oceanog-
365 raphy*, **45** (4), 1174–1188, doi:10.1175/JPO-D-14-0167.1, URL [http://dx.doi.org/10.1175/
366 JPO-D-14-0167.1](http://dx.doi.org/10.1175/JPO-D-14-0167.1).
- 367 Whalen, C. B., L. D. Talley, and J. A. MacKinnon, 2012: Spatial and temporal variabil-
368 ity of global ocean mixing inferred from argo profiles. *Geophys. Res. Lett.*, **39** (L18612),
369 doi:10.1029/2012GL053196.
- 370 ~~Portion of a CTD cast showing depth vs time (top) for a portion of an upcast, with data flagged
371 as loops in red. Lower panel shows corresponding xpod timeseries of dT/dt for that time with
372 discarded loop data in red. Note that variance tends to be larger during depth loops due to entrained
373 water and CTD-induced turbulence.~~

LIST OF FIGURES

374	Fig. 1. Photo of CTD rosette during EQ14 with χ - pods -pods attached.	22
376	Fig. 2. Ratio of the maximum observed wavenumber $k_{max} = f_{max}/u$ to the Batchelor wavenumber k_b for different values of ϵ , assuming a $f_{max} = 7\text{Hz}$. Each line is for a different flowspeed.	23
378	Fig. 3. Example timeseries from one CTD cast during EQ14. a) CTD pressure. b) Fallspeed of CTD (dp/dt) .c) Vertical and horizontal accelerations measured by χ - pod -pod. d) Temperature from CTD and (calibrated) χ - pod -pod sensors. T2 is offset slightly for visualization. e) Temperature derivative dT/dt measured by the upward-looking χ - pod -pod sensor T1. f) Temperature derivative dT/dt measured by the downward-looking χ - pod -pod sensor T2.	24
383	Fig. 4. Portion of a CTD cast showing depth vs time (top) for a portion of an upcast, with data flagged as loops in red. Lower panel shows corresponding χ -pod timeseries of dT/dt for that time with discarded loop data in red. Note that variance tends to be larger during depth loops due to entrained water and CTD-induced turbulence.	25
387	Fig. 5. Example temperature gradient spectra from EQ14, for high (top) and low (bottom) ϵ . Solid black line with circles show the observed spectra. Dashed line shows the fitted theoretical Kraichnan spectra for the χ -pod estimates. Magenta line is Kraichnan spectra for Chameleon χ and ϵ measured at the same depth. Vertical dashed blue(red) lines indicate the minimum (maximum) wavenumber used in the χ -pod calculation. The Batchelor wavenumber k_b is also indicated by the vertical cyan line.	26
393	Fig. 6. Depth-time plots of $\log_{10}\chi$ from both methods for EQ14 data. Top: χ -pod method. Black diamonds indicate casts used for comparison with CTD- χ -pod profiles. Bottom: Chameleon.	27
395	Fig. 7. Left: 2D histogram of $\log_{10}(\chi)$ from Chameleon (x-axis) and χ -pod method (y-axes). Values from each profile were averaged in the same 5m depth bins. Right: Normalized histogram of $\log_{10}[\chi_\chi/\chi_\epsilon]$. Vertical dashed line indicates the mean of the distribution.	28
398	Fig. 8. Left: Scatter plot of χ from CTD- χ -pod profiles versus the mean of bracketing Chameleon profiles. Black dashed line shows 1:1, red are $\pm 10\chi$. Right: Normalized histogram of the log of ratios.	29
401	Fig. 9. Histogram of \log_{10} of the ratio of χ for nearby casts. The first set is for the before (cham1) and after (cham2) Chameleon profiles. the 2nd is CTD- χ -pod profiles versus the before(cham1) profiles. The last is CTD- χ -pod profiles versus the after(cham2) profiles. Dashed lines show the medians of each set. Note that bias is small/zero, and the variability (spread) between CTD/cham is similar to the natural variability between cham profiles.	30
406	Fig. 10. Time mean of χ for all CTD- χ -pod - Chameleon cast pairs, with 95% bootstrap confidence intervals.	31
408	Fig. 11. Histogram of % error for χ computed with constant added to fallspeed, in order to examine sensitivity to fallspeed.	32
410	Fig. 12. Left: 2D histograms of χ computed using the iterative χ - pod -pod method (top) and the MLE fit (bottom) versus χ computed from Chameleon. Note that the MLE method underestimates χ at larger magnitudes. Right: Histograms of the log of ratios for different ranges of ϵ	33

34

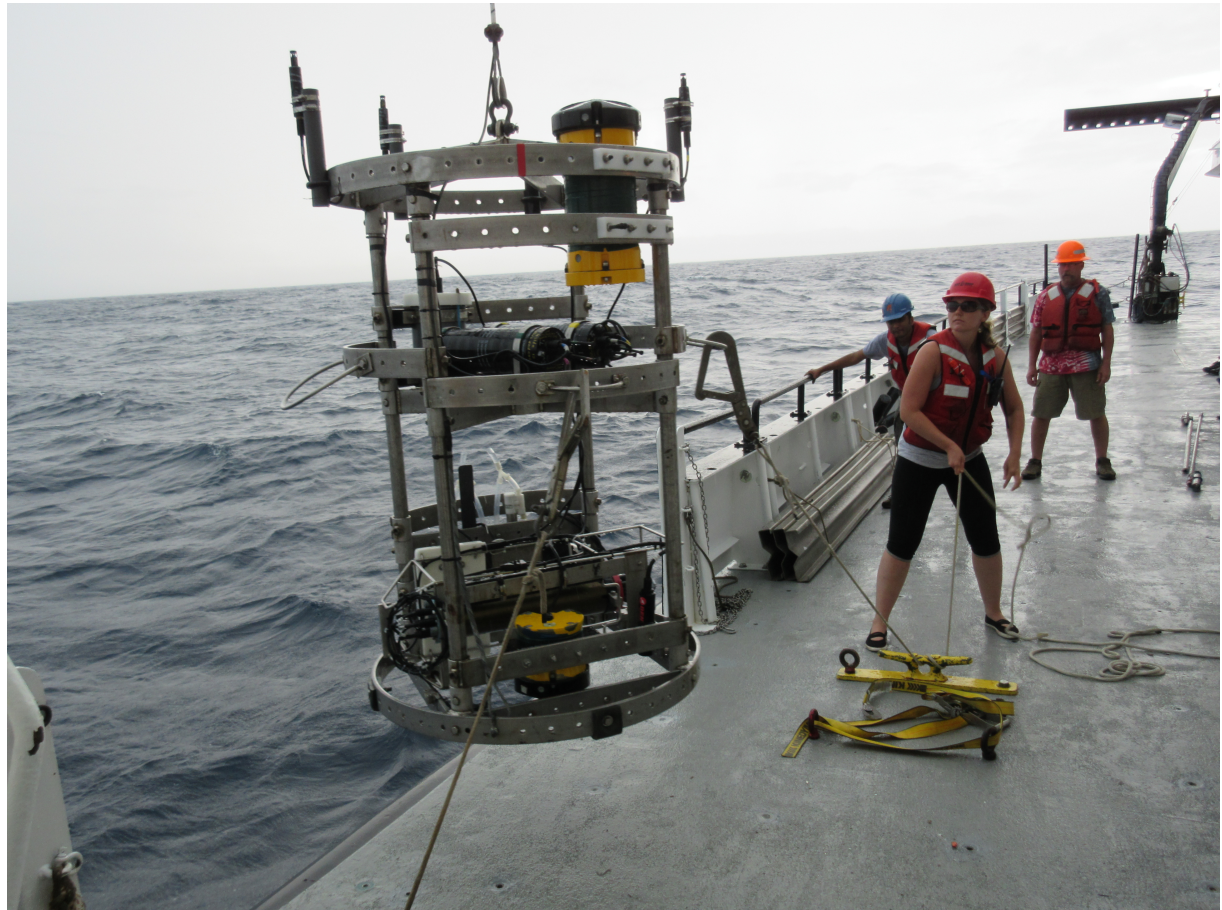
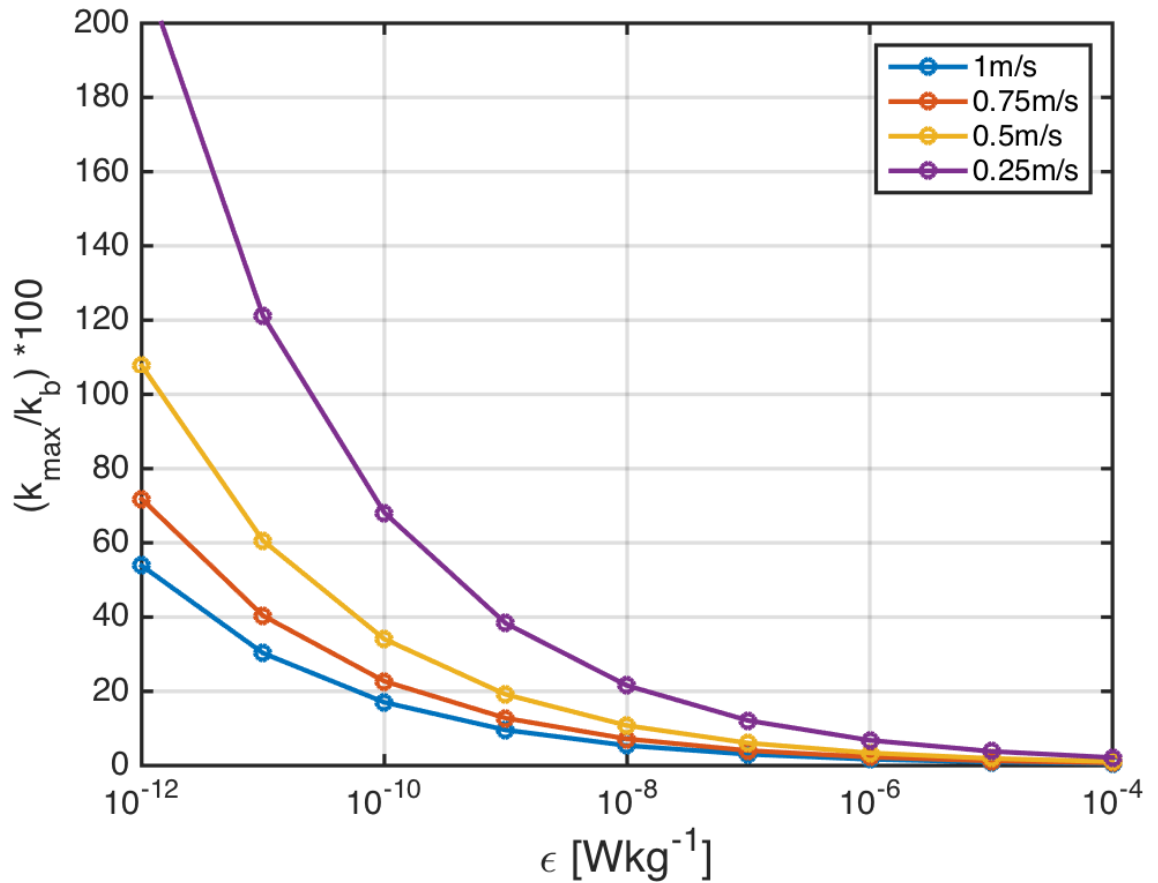
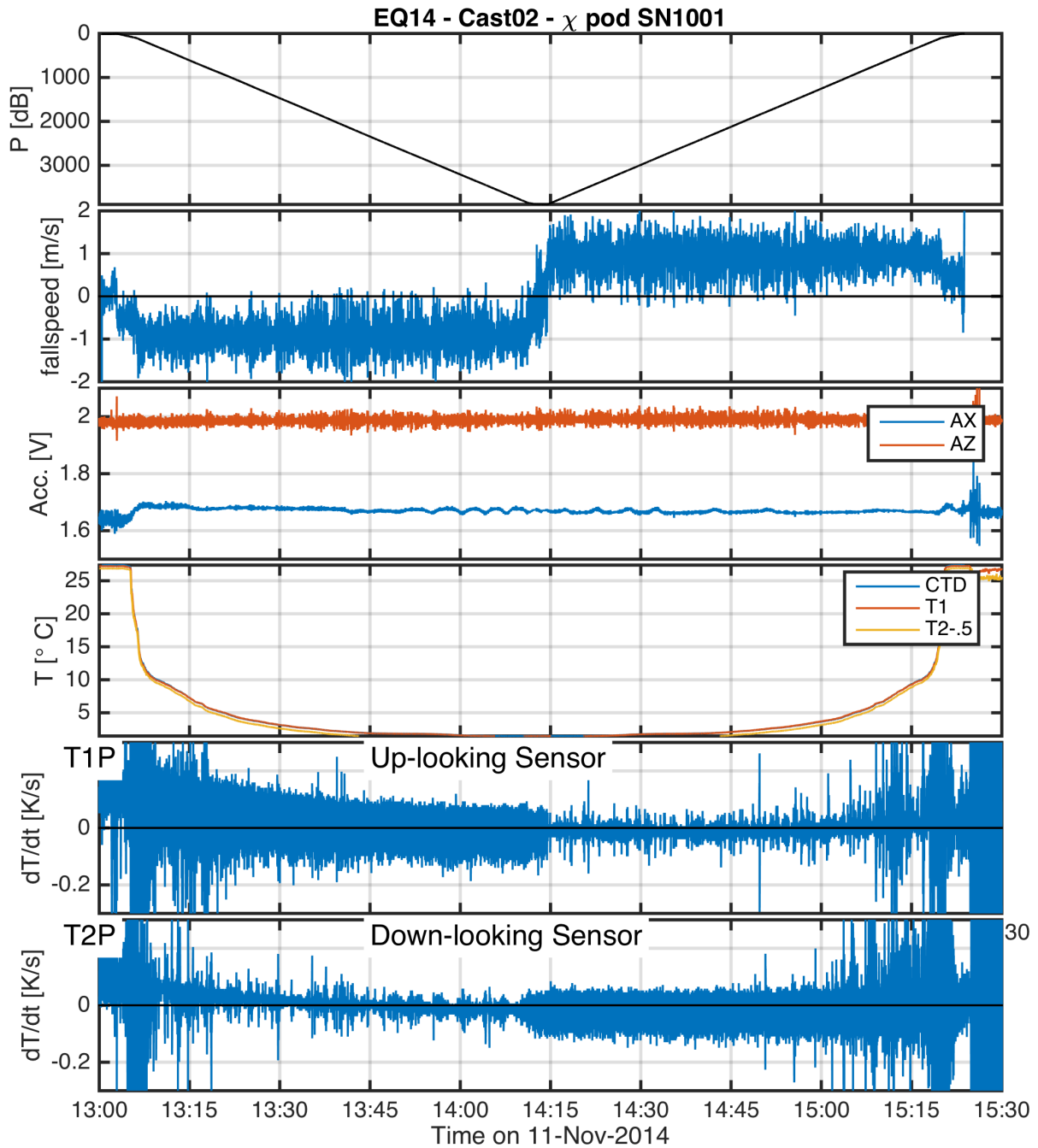


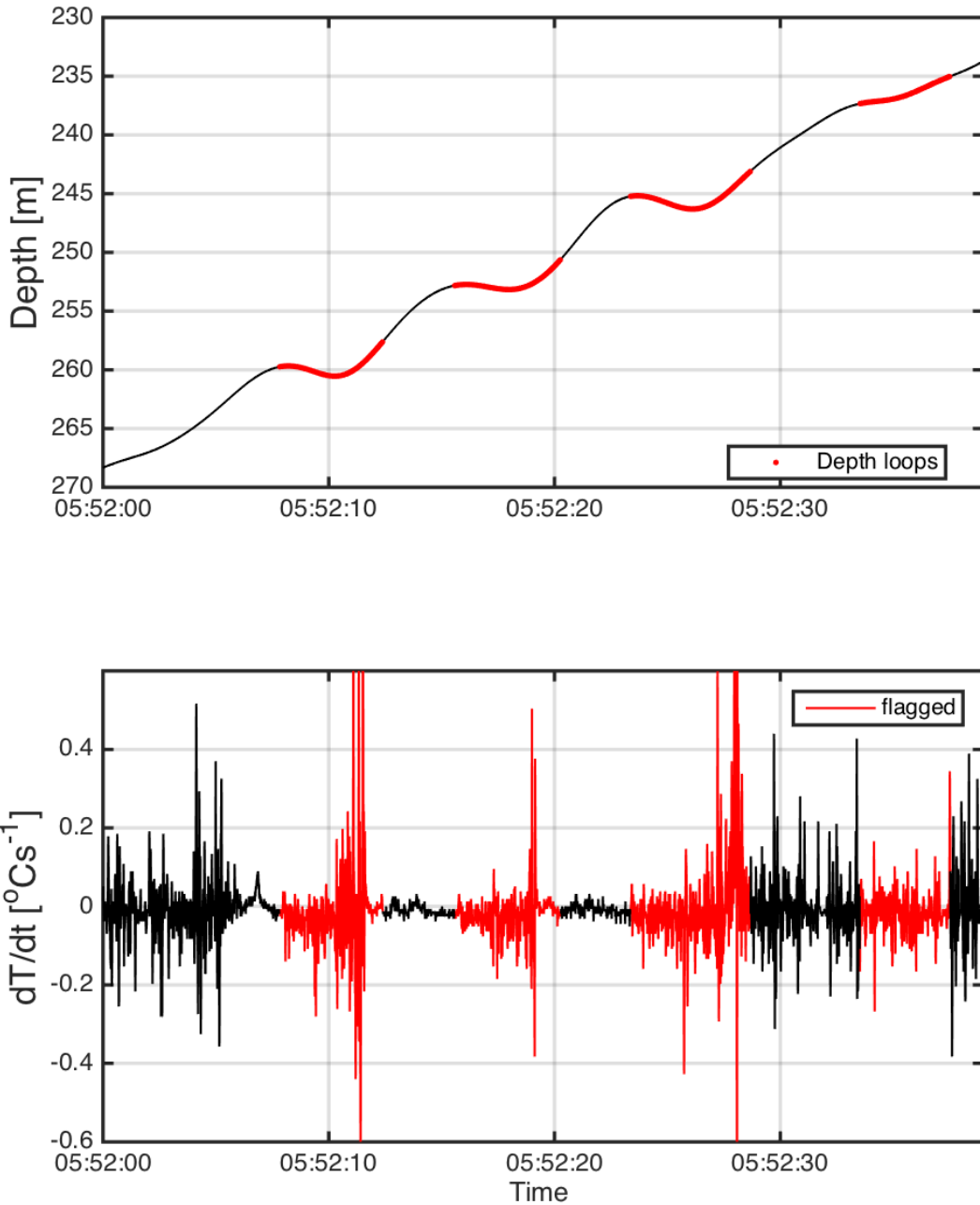
FIG. 1. Photo of CTD rosette during EQ14 with χ -**ped**s-pods attached.



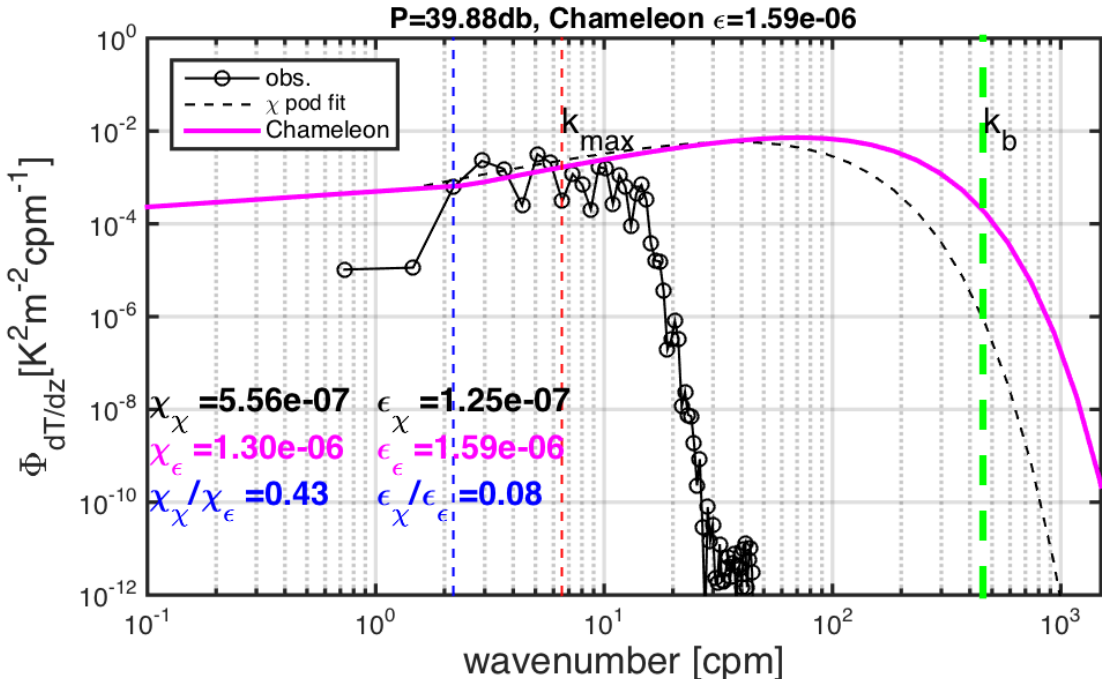
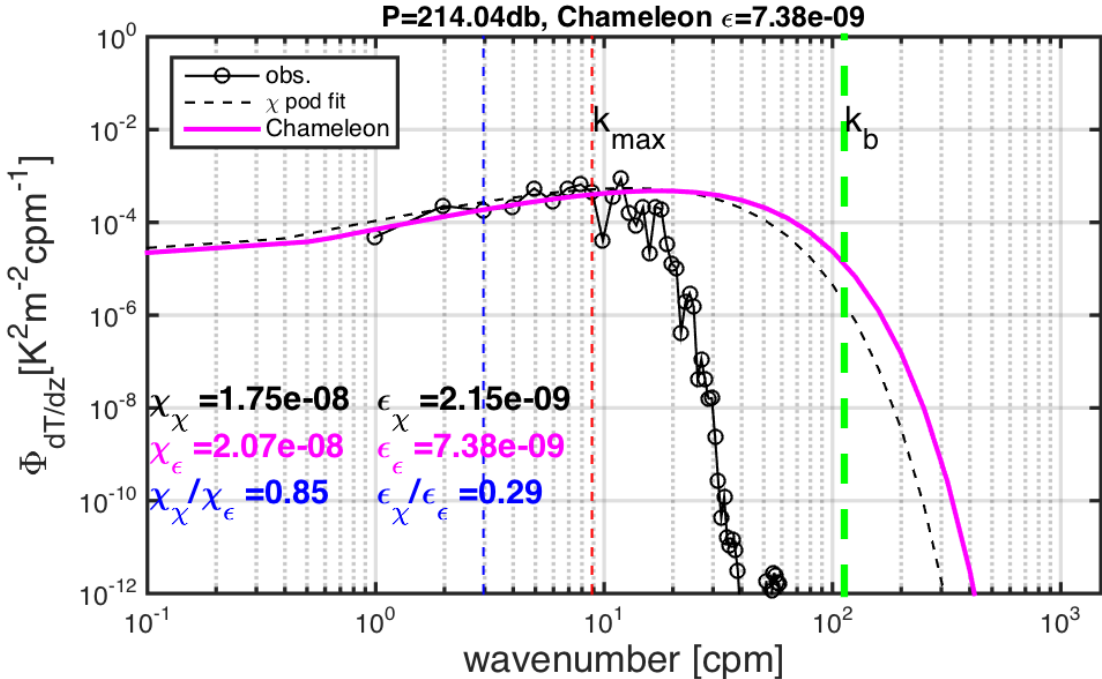
418 FIG. 2. Ratio of the maximum observed wavenumber $k_{\max} = f_{\max}/u$ to the Bachelor wavenumber k_b for
 419 different values of ϵ , assuming a $f_{\max} = 7\text{Hz}$. Each line is for a different flowspeed.



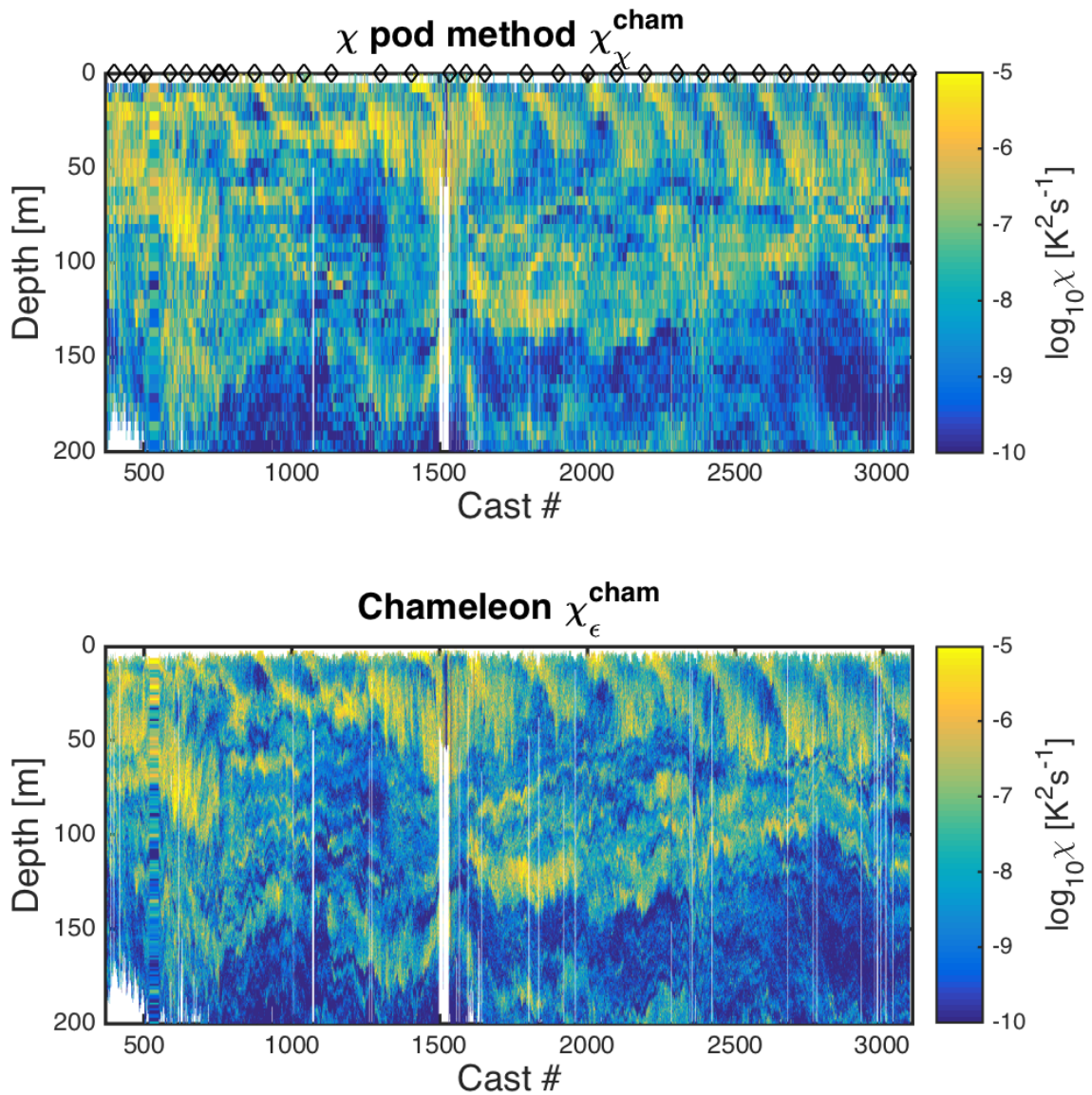
420 FIG. 3. Example timeseries from one CTD cast during EQ14. a) CTD pressure. b) Fallspeed of CTD (dp/dt)
 421 .c) Vertical and horizontal accelerations measured by χ -pod. d) Temperature from CTD and (calibrated)
 422 χ -pod sensors. T2 is offset slightly for visualization. e) Temperature derivative dT/dt measured by the
 423 upward-looking χ -pod sensor T1. f) Temperature derivative dT/dt measured by the downward-looking
 424 χ -pod sensor T2.



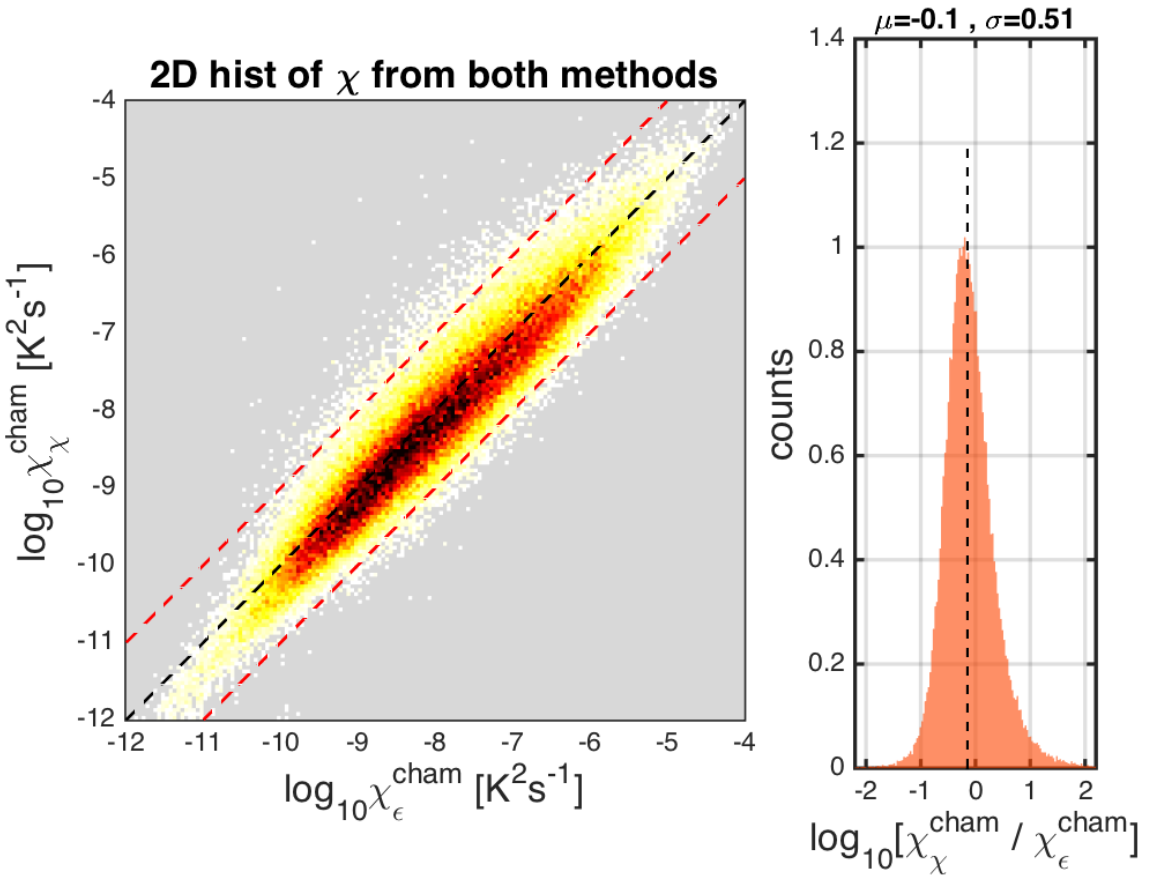
425 FIG. 4. Portion of a CTD cast showing depth vs time (top) for a portion of an upcast, with data flagged as
 426 loops in red. Lower panel shows corresponding χ_{pod} timeseries of dT/dt for that time with discarded loop
 427 data in red. Note that variance tends to be larger during depth loops due to entrained water and CTD-induced
 428 turbulence.



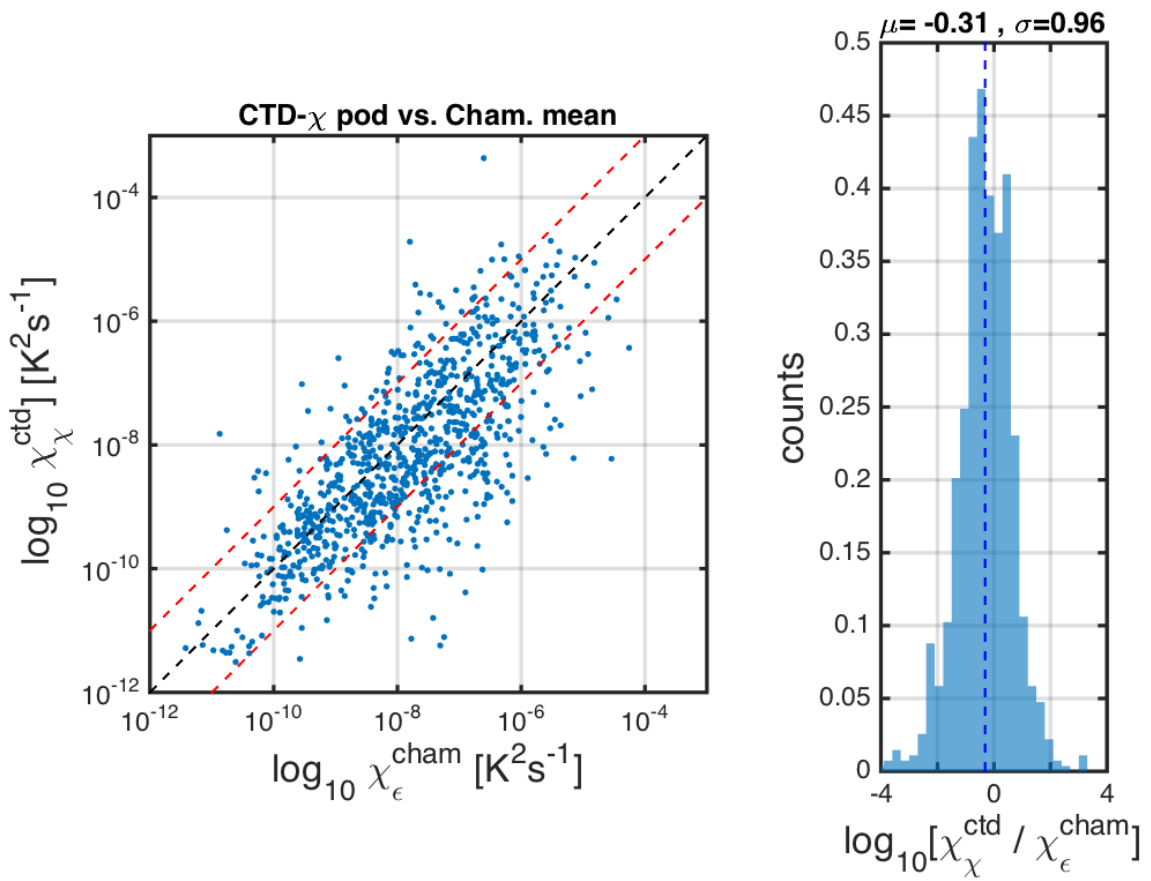
429 FIG. 5. Example temperature gradient spectra from EQ14, for high (top) and low (bottom) ϵ . Solid black
430 line with circles show the observed spectra. Dashed line shows the fitted theoretical Kraichnan spectra for
431 the χ pod estimates. Magenta line is Kraichnan spectra for Chameleon χ and ϵ measured at the same depth.
432 Vertical dashed blue(red) lines indicate the minimum (maximum) wavenumber used in the χ pod calculation.
433 The Batchelor wavenumber k_b is also indicated by the vertical cyan line.



434 FIG. 6. Depth-time plots of $\log_{10}\chi$ from both methods for EQ14 data. Top: χ pod method. Black diamonds
 435 indicate casts used for comparison with CTD- χ pod profiles. Bottom: Chameleon.



436 FIG. 7. Left: 2D histogram of $\log_{10}(\chi)$ from Chameleon (x-axis) and χ_{pod} method (y-axes). Values from
 437 each profile were averaged in the same 5m depth bins. Right: Normalized histogram of $\log_{10}[\chi_{\chi}/\chi_{\epsilon}]$. Vertical
 438 dashed line indicates the mean of the the distribution.



439 FIG. 8. Left: Scatter plot of χ from CTD- χ pod profiles versus the mean of bracketing Chameleon profiles.
440 Black dashed line shows 1:1, red are ± 10 X. Right: Normalized histogram of the log of ratios.

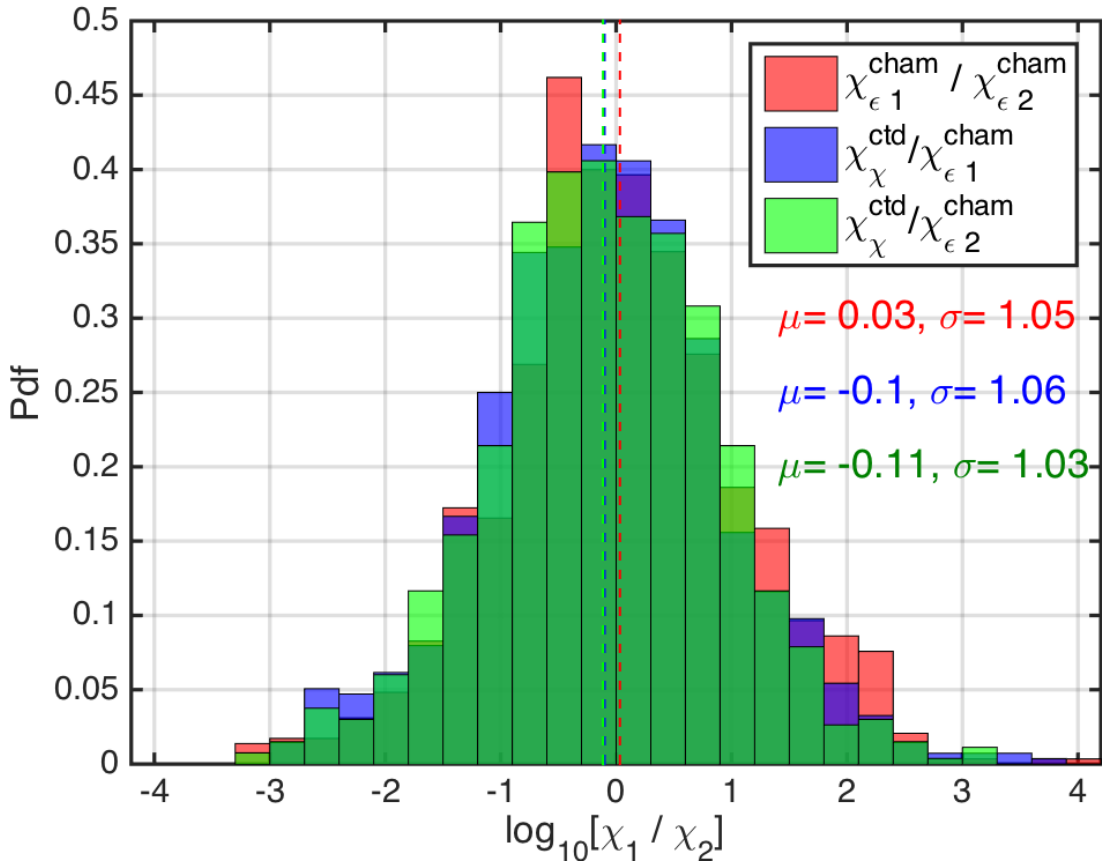


FIG. 9. Histogram of \log_{10} of the ratio of χ for nearby casts. The first set is for the before (cham1) and after (cham2) Chameleon profiles. the 2nd is CTD- χ pod profiles versus the before(cham1) profiles. The last is CTD- χ pod profiles versus the after(cham2) profiles. Dashed lines show the medians of each set. Note that bias is small/zero, and the variability (spread) between CTD/cham is similar to the natural variability between cham profiles.

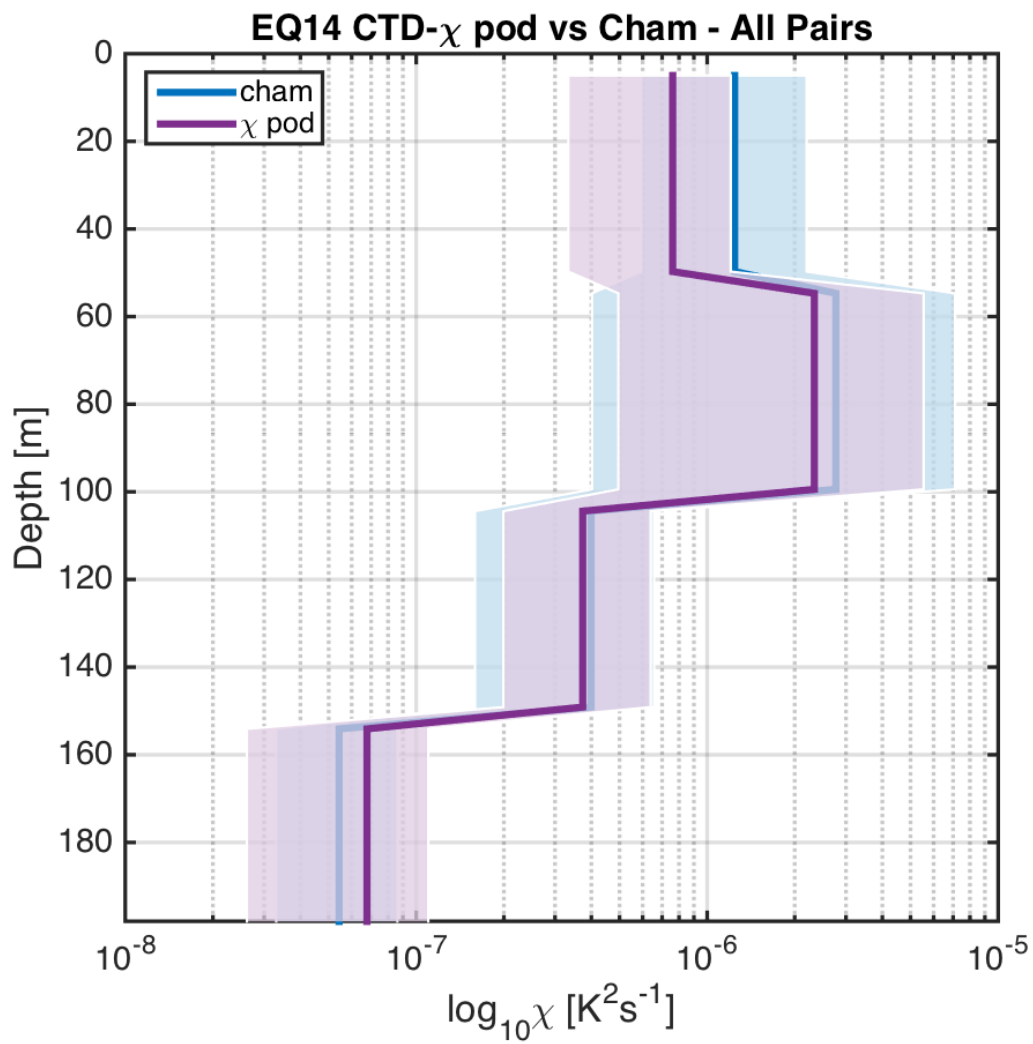
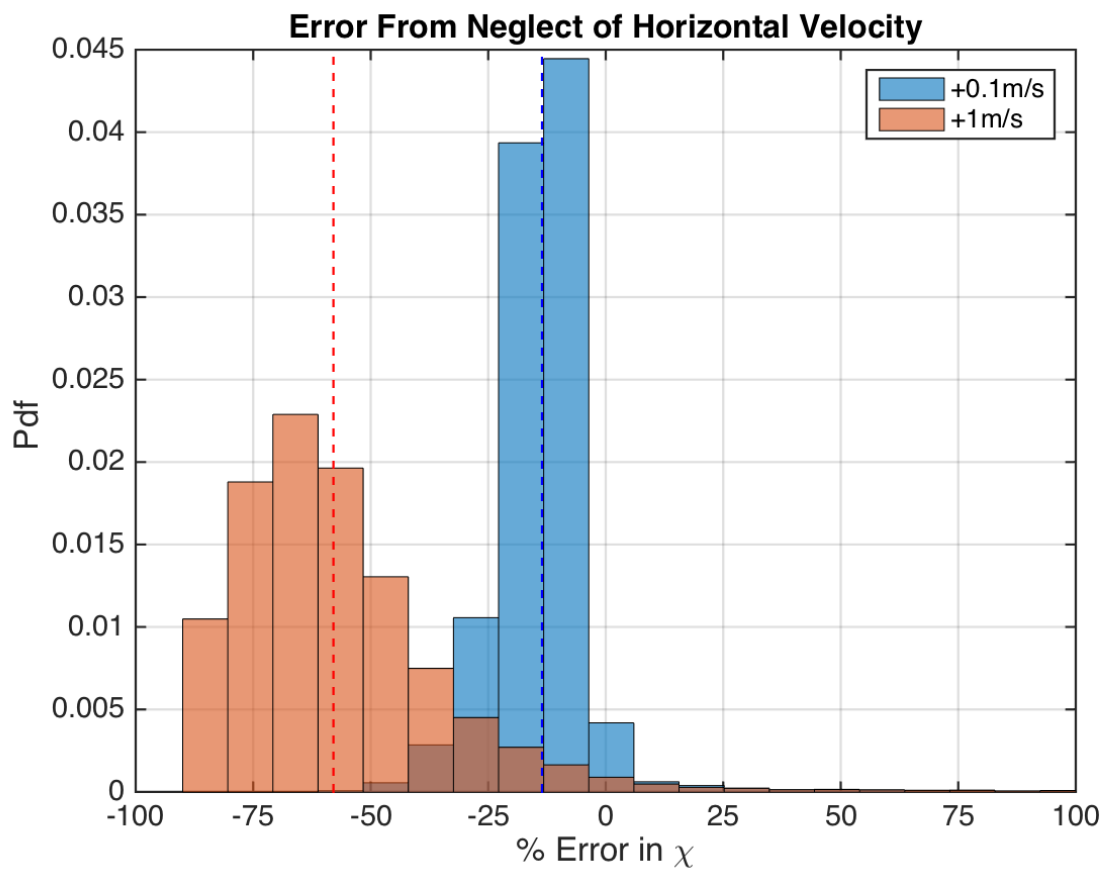
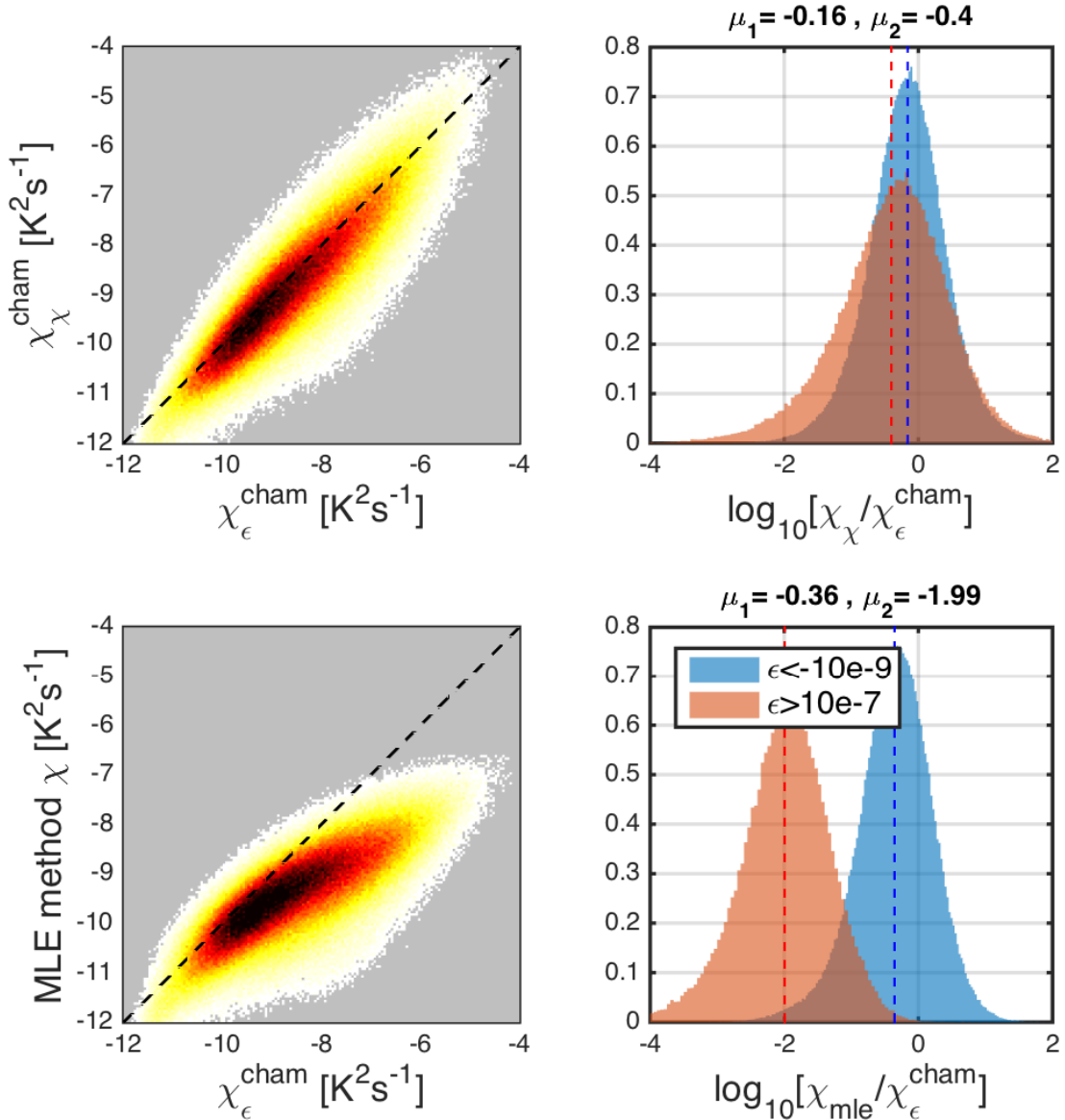


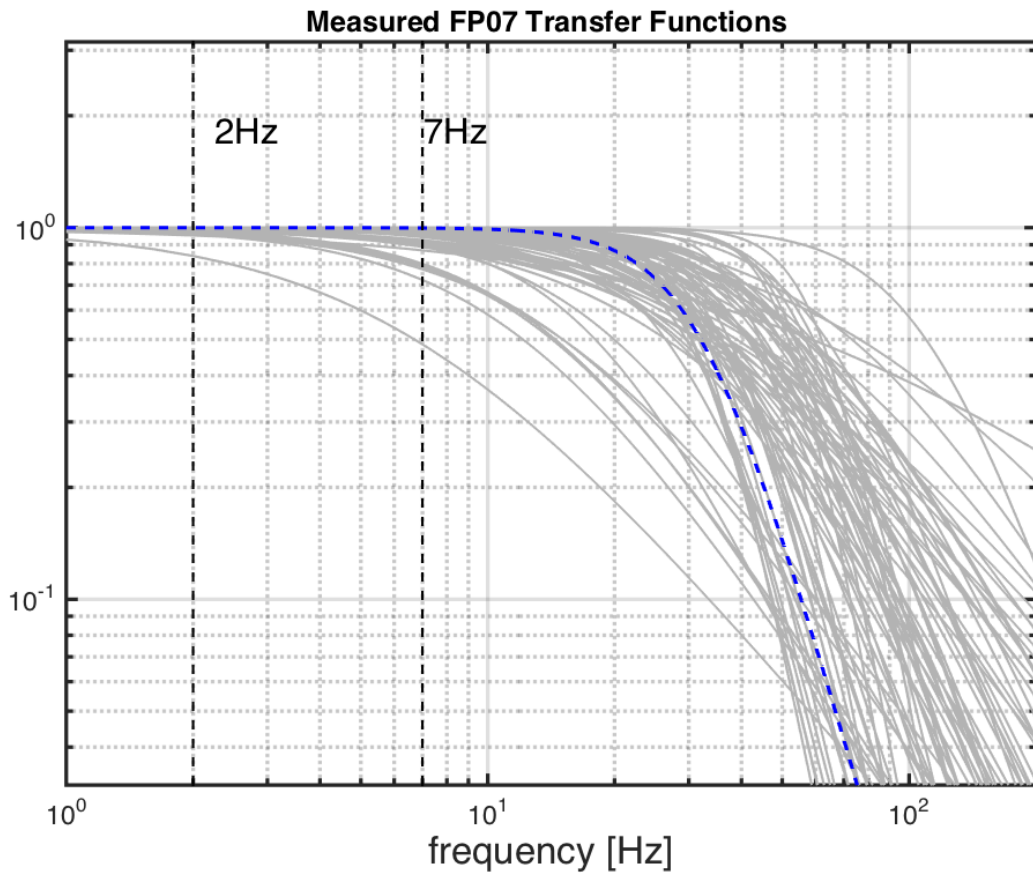
FIG. 10. Time mean of χ for all CTD- χ pod - Chameleon cast pairs, with 95% bootstrap confidence intervals.



446 FIG. 11. Histogram of % error for χ computed with constant added to fallspeed, in order to examine sensitivity
447 to fallspeed.



448 FIG. 12. Left: 2D histograms of χ computed using the interative χ -~~pod~~-pod method (top) and the MLE fit
 449 (bottom) versus χ computed from Chameleon. Note that the MLE method underestimates χ at larger magni-
 450 tudes. Right: Histograms of the log of ratios for different ranges of ϵ .



451 FIG. 13. Measured FP07 thermistor transfer functions from historical database. Vertical dashed lines show
 452 the frequency range used in χ pod method. Dashed blue line is a generic transfer function found to best match
 453 measured functions, and is used when response functions are no longer measured.